PAPER

Check for updates

Establishing empirical design rules of nucleic acid templates for the synthesis of silver nanoclusters with tunable photoluminescence and functionalities towards targeted bioimaging applications†

Jason Y. C. Lim, [ID] ‡[a] Yong Yu, [ID] ‡[a] Guorui Jin,[a] Kai Li, [ID][a] Yi Lu, [ID][b] Jianping Xie [ID][c] and Yen Nee Tan [ID] *[ad]

DNA-templated silver nanoclusters (AgNCs) are an emerging class of ultrasmall (<2 nm) fluorophores with increasing popularity for bioimaging due to their facile synthesis and tunable emission color. However, design rules correlating different nucleotide sequences with the photoemission properties of AgNCs are still largely unknown, preventing the rational design of DNA templates to fine-tune the emission color, brightness and functionalities of AgNCs for any targeted applications. Herein, we report a systematic investigation to understand the empirical influences of the four basic DNA nucleotides on AgNC synthesis and their effects on photoluminescence properties. After establishing the importance of nucleotide−Ag$^+$ binding and AgNC encapsulation within DNA tetraplex structures, we then determined the unique attributes of each individual nucleobase using different combinations of systematically varied DNA templates. Using the empirical design rules established herein, we were able to predict the photoluminescence behaviours of AgNCs templated by complex aptamer sequences with specific binding affinity to human cancer cells, and to deliberately control their emission color by rational modifications of the DNA template sequences for targeted bioimaging. Our empirical findings from this systematic experimentation can contribute towards the rational design of DNA sequences to customise the photoluminescence properties and biofunctionalities of DNA-protected AgNCs towards multicolour targeted bioimaging applications.

1. Introduction

Nucleic acids such as DNA are one of the most important biological macromolecules in nature, responsible for the storage and transmission of genetic information as well as regulation of many biological processes. Structurally consisting of only four universal nucleotides (*i.e.*, adenine, thymine, cytosine and guanine), their specific permutations determine the conformations, and supramolecular structures, as well as the chemical and biological properties of DNA. Due to the ease of sequence tunability and well-understood base-pairing properties, DNA molecules can be synthetically designed at high precision and produced at low cost, leading to diverse application of DNA in biomedicine (*e.g.*, biomarkers for diseases diagnostics), materials science (*e.g.*, self-assembled DNA origami), electronics (*e.g.*, DNA logic gates), and computing.[1–4] More recently, the realization that biomolecules can also act as precursors (to form nanodots),[5–10] and capping or reducing agents for the coordination of metal cations has revolutionized the field of bionanotechnology,[11,12] opening up new opportunities to produce exotic biohybrid nanomaterials such as DNA-assembled metal nanostructures,[13–16] DNA-/peptide-synthesized anisotropic metal nanoparticles,[17–21] protein-/peptide-templated ultrasmall metal nanoclusters,[22–27] and even nucleotide-derived nanodots (without metal precursors),[7] which inherit not only the biocompatibility and functionality of biomolecules, but also possess unique physiochemical properties of nanomaterials for a wide range of technological applications.[11,28–30]

Since the seminal work of using DNA molecules as stabilizers (or templates) to form photoluminescent silver nanoclusters (AgNCs) by Dickson and coworkers in 2004,[31] the fundamental

[a]Institute of Materials Research and Engineering, The Agency for Science, Technology and Research (A*STAR), 2 Fusionopolis Way, #08-03, Innovis, 138634, Singapore

[b]Department of Chemistry, University of Illinois at Urbana-Champaign, Urbana, IL 61801, United States

[c]Department of Chemical and Biomolecular Engineering, National University of Singapore, 10 Kent Ridge Crescent, 119260, Singapore

[d]Faculty of Science, Agriculture & Engineering, Newcastle University, Newcastle Upon Tyne NE1 7RU, UK. E-mail: yennee.tan@newcastle.ac.uk

† Electronic supplementary information (ESI) available. See DOI: 10.1039/d0na00381f

‡ J. Y. C. L. and Y. Y. contributed equally to this work.

study and applications of DNA-templated AgNCs (DNA-AgNCs) have witnessed dramatic advancements in recent years.[32–36] These DNA-AgNCs are typically smaller than 2 nm,[37] approaching the Fermi wavelength of electrons. Due to strong quantum confinement, the continuous density of states present in the bulk metals are broken up into discrete energy levels which give rise to optical, electrical and chemical properties distinctly different from those of the bulk metal and metal nanoparticles of larger sizes.[38] While AgNCs can also be produced using templates such as zeolites,[39–41] organic polymers,[42–44] thiols,[45–51] sugar molecules,[52] and peptides,[53–55] DNA-AgNCs are especially valued for biological applications due to their biological and physicochemical properties. DNA-AgNCs are highly biocompatible, possess generally good photostability, are easy to synthesize using environmentally-benign reagents, and possess high versatility for tuning their photophysical properties, including photoemission color and brightness, across the entire range of the visible and near-IR spectrum by simply varying the nucleotide sequences of the DNA templates. They are important alternatives to traditional organic fluorophores and inorganic quantum dots as organic fluorophores often require multi-stepped chemical syntheses and are susceptible to photobleaching,[56] while quantum dots can pose cytotoxicity concerns.[57,58]

A huge repertoire of AgNCs with widely varying photophysical properties are currently known,[35] with those templated by poly-cytosine sequences[59] being arguably the most thoroughly studied. However, to date, the ability to predict AgNC emission colors *a priori* from simply knowing the templating DNA sequence still remains unrealized. This is due to the numerous complexities preventing a full elucidation of these design rules. For example, DNA molecules can self-assemble and adopt supramolecular structures in solution, each nucleobase has different inherent affinities for silver, the great variety of geometries and atomic compositions of AgNCs,[60] and even electron-transfer interactions between nucleobases and AgNCs,[61] just to name a few. Traditionally, identifying suitable DNA molecules to template the formation of AgNCs with different photoluminescence colors relied on the trial-and-error screening of DNA libraries.[62,63] More recently, machine learning and data mining approaches have been exploited to better predict how different templating sequences can affect the AgNC emission colors with greater precision and accuracy.[64,65] Nevertheless, a systematic empirical approach to elucidate these coveted design rules by studying the effects of methodologically changing combinations of nucleobases on the DNA template has yet to be demonstrated.

In this study, we report a systematic empirical investigation on the design principles of ssDNA sequences to rationally tune the photoemission colors of AgNCs. Compared to hybridized DNA templates such as DNA hairpin loops and double-stranded DNA for AgNC templating, ssDNA templates are more versatile due to their conformational flexibility which allow exposure of most if not all the nucleobases present in the DNA template for easy coordination and interaction with silver cations or AgNCs. While this ensures higher binding affinities and potentially greater AgNC stabilization by simultaneous binding to multiple

nucleobases, ssDNA templates also allow better fundamental understanding of how different DNA nucleobases affect the photoluminescence of the resultant AgNCs by eliminating additional complications arising from structural features such as loops or hairpins, despite their known ability to also template photoluminescent AgNCs.[66] For our empirical study, we first established the fundamental influence exerted by each nucleobase on AgNC formation using four homo-oligonucleotides containing 20 cytosines, guanines, adenines or thymines, denoted as dC_{20}, dG_{20}, dA_{20} and dT_{20}, respectively, as templates of AgNCs. We then studied the effects of introducing a second nucleobase into the DNA sequence by systematically changing their relative proportions in the sequence. These dual-block DNA sequences contain combinations of two nucleobases with the general formula of $d[X_{5n}Y_{(20-5n)}]$, where n is an integer from 0 to 4 and X and Y are any two of the four possible nucleotides (A, T, C, and G). Intriguingly, we found that each of the four nucleobases exert their own characteristic influences on the photoluminescence properties of AgNCs. Thereafter, to confirm the importance of having consecutive homonucleotide sequences for formation of bright-luminescent AgNCs, we studied the effects of using interdigitated sequences containing two nucleobases, bearing the general formula $d[XY]_{10}$. Importantly, we evaluate the influence of different nucleobase combinations on time-dependent variations in AgNC emissive properties – a factor hitherto not considered in the vast majority of these studies. We then validated the empirical rules we have established by predicting the photoluminescence properties of AgNCs templated by several complex long aptamer sequences (41–77 mers) containing all four nucleobases. These design rules also facilitated our design of bi-functional DNA templates by incorporating cancer cell specific aptamer sequences, leading to the formation of bright photoluminescent DNA-AgNCs with a tailored emissive color and cell-targeting capabilities for cancer diagnostics. Our systematic empirical approach can complement existing high-throughput screening and data-analytical methods to better understand how the photoluminescence properties of AgNCs can be influenced by a specific templating DNA sequence.

2. Results and discussion

2.1. Pre-requisites for photoluminsecent DNA-templated silver nanocluster formation

Firstly, four homo-oligonucleotides with fixed length of 20 bases, *i.e.* homo-adenine (dA_{20}), homo-tymine (dT_{20}), homo-guanine (dG_{20}), and homo-cytosine (dC_{20}), were used as templates to elucidate the essential structural features of DNA for the formation of photoluminescent silver nanoclusters (AgNCs). Fig. 1 shows the time evolution photoluminescence profiles (left panel) of AgNCs templated by the respective homo-oligonucleotides. In the presence of dA_{20} or dT_{20}, no AgNCs were formed upon the chemical reduction of the silver nitrate precursor by sodium borohydride ($NaBH_4$) after an initial incubation period of 20 minutes. At 24 hours, the dT_{20}-templated sample remained non-emissive (Fig. 1A), while spectroscopically-pure ($\lambda_{ex} = 440$ nm/$\lambda_{em} = 520$ nm) and weakly-
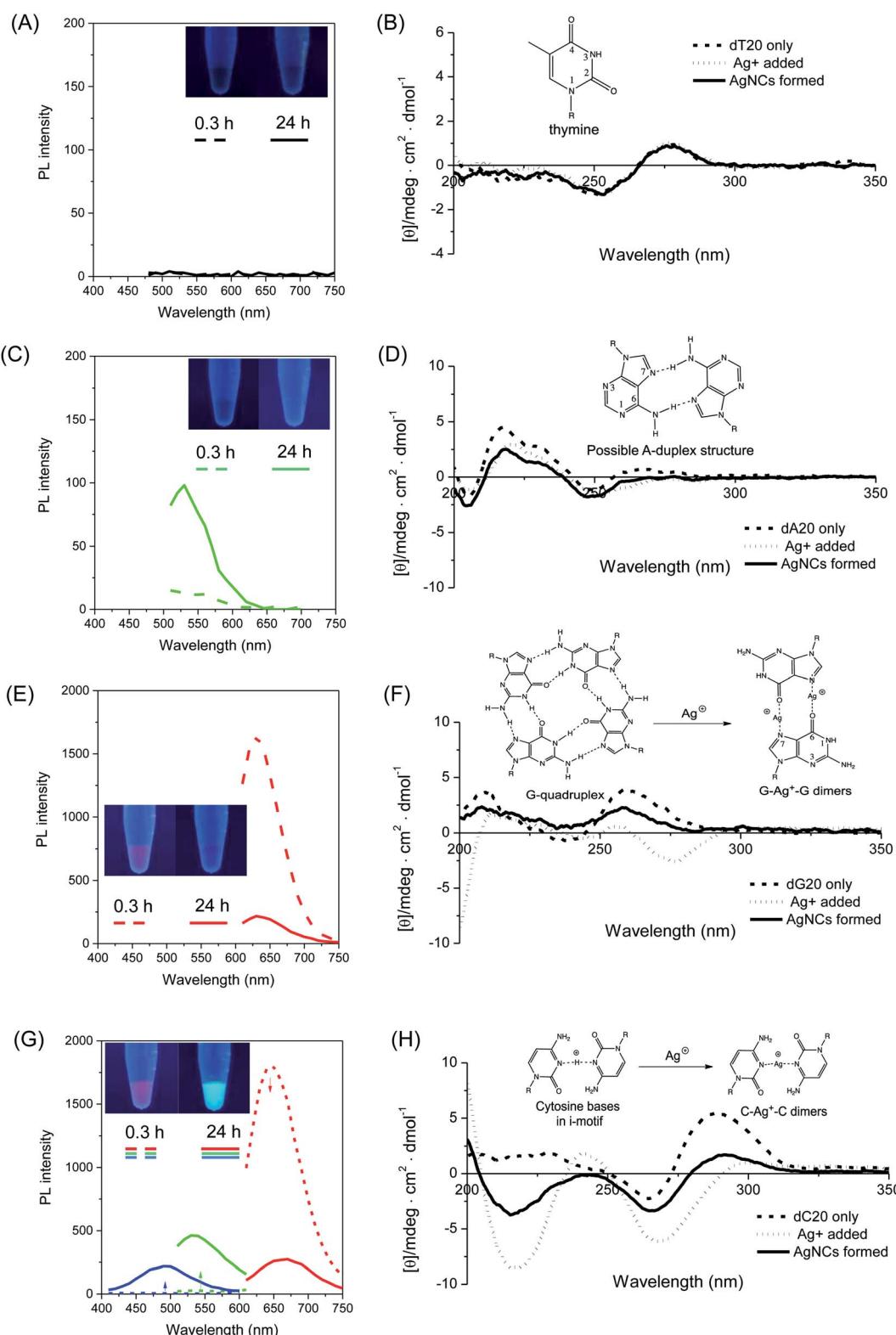
Fig. 1 (Left panel) Photoluminescence spectra of freshly prepared ($t = 0.3$ h, dash lines) and aged ($t = 24$ h, solid lines) AgNCs templated by (A) dT_{20} ($\lambda_{ex} = 440$ nm), (C) dA_{20} ($\lambda_{ex} = 440$ nm), (E) dG_{20} ($\lambda_{ex} = 570$ nm) and (G) dC_{20} DNA sequences. The blue, green and red emission spectra in (G) were obtained at excitation wavelengths (λ_{ex}) of 340, 450 and 580 nm respectively. (Inset) Digital photos of respective AgNCs under UV illumination obtained at 0.3 h and 24 h respectively. (Right panel) Circular dichroism spectra showing the structural changes (inset) occurring in the respective homo-nucleobase DNA sequences (B: dT_{20}, D: dA_{20}, F: dG_{20}, H: dC_{20}).

luminescent green emissive AgNCs were formed in the presence of the dA_{20} template (Fig. 1C). As shown in Fig. 1E, the dG_{20} template produced red-emitting AgNCs in 20 minutes (λ_{ex} = 570 nm/λ_{em} = 630 nm), whose photoluminescence (PL) intensity decreased with time and no other emitter was formed in the process. While the dC_{20} template also formed red-emitting AgNCs (λ_{ex} = 580 nm/λ_{em} = 670 nm) initially, a time-dependent color conversion of dC_{20}-AgNCs to green- (λ_{ex} = 440 nm/λ_{em} = 540 nm) and blue-emitting (λ_{ex} = 340 nm/λ_{em} = 490 nm) species was observed after 24 hours of incubation, giving detectable emission color changes (inset in Fig. 1G). Interestingly, cytosine and guanine, which formed bright emissive AgNCs in this study, were found to bind strongly to the silver precursor (Ag^+), as determined by the isothermal titration calorimetric (ITC) studies reported by Sastry *et al.*[67] The same study also showed that the binding of thymine, which did not form photoluminescent AgNCs, to Ag^+ was the weakest. This highlights the importance of nucleobase–Ag^+ binding in forming photoluminescent AgNCs.

To investigate the functional roles of DNA templates in the synthesis of AgNCs, circular dichroism (CD) spectroscopy was employed to obtain some mechanistic insights into the structural changes of DNA templates in the process of AgNC formation. Thus, the CD spectra of the respective DNA templates were recorded at various stages of AgNC formation as shown in Fig. 1 (right panel), *i.e.*, before (dashed line) and after addition (dotted line) of silver nitrate, as well as 20 minutes after addition of $NaBH_4$ to form the AgNCs (solid lines). Similar to the PL spectrum, no detectable changes in the CD spectra of dT_{20} templates were observed upon addition of Ag^+, and after $NaBH_4$ reduction, with all three spectra practically superimposable on each other (Fig. 1B). For the dA_{20} template, a positive peak at *ca.* 220 nm was observed in its CD spectrum (Fig. 1D, dashed line), suggesting the presence of self-assembled supramolecular structures, such as adenine–adenine dimers in solution.[68] Subsequently, the binding of Ag^+ and its reduction by $NaBH_4$ caused marginal, but detectable changes to its CD spectra, implying that only small structural changes in the DNA template occurred during these processes. These findings indicated that both the dT_{20} and dA_{20} sequences interact weakly with Ag^+ and Ag^0 at neutral pH, in accordance with our aforementioned findings that they act as poor templates for the formation of photoluminescent AgNCs.

In stark contrast, the homo-oligonucleotide sequences which are capable of forming bright emissive AgNCs (*i.e.*, dC_{20} and dG_{20}) showed dramatic changes in their CD spectra during the AgNC formation process. For instance, the CD spectra of dG_{20} exhibited a positive peak at 260 nm and a negative peak at 240 nm (Fig. 1F, dashed line), indicating the parallel-stranded G-quadruplex structures where the individual oligo-guanine strands formed tetrameric structures *via* Hoogsteen base pairing in solution.[69–72] When Ag^+ was added, the characteristic peaks of the G-quadruplex structure disappeared, accompanied with the appearance of a new prominent peak at a negative ellipticity of 275 nm (Fig. 1F, dotted line). This observation strongly implies the significant disruption of the G-quadruplex structure upon Ag^+ binding, probably due to the formation of

guanine–Ag^+–guanine dimers,[73] which is consistent with the strong guanine–Ag^+ binding affinity.[67] Interestingly, upon chemical reduction of Ag^+, the original peaks at 240 nm and 260 nm re-appeared in the CD spectrum (Fig. 1F, solid line), suggesting that the G-quadruplex structure of the dG_{20} template was restored to some extent in solution following the release of Ag^+ from the binding sites to form AgNCs, thus freeing the guanine ligands for re-formation of the G-quadruplex structures. Owing to their hydrophobicity, the as-synthesized AgNCs are likely to be encapsulated within the hydrophobic interior of the reformed G-quadruplex scaffolds. This process most likely stabilizes the as-formed AgNCs against various photoluminescence quenching pathways in solution, resulting in the high brightness of red emissive dG_{20}-AgNCs as observed in this study. As shown in Fig. 1H (dashed line), the CD spectrum of dC_{20} alone displayed a positive peak at 285 nm, which is a signature of i-motif tetraplex structures in solution.[74] However, the introduction of Ag^+ resulted in the loss of this characteristic peak with simultaneous appearance of two negative peaks at 220 nm and 265 nm (Fig. 1H, dotted line), suggesting the binding of cytosine bases to Ag^+. Concomitantly, this process led to a severe disruption of the original i-motif structure, possibly arising from the coordination of cytosine bases to Ag^+ to form cytosine–Ag^+–cytosine dimers[75] that tilted the bases relative to the helical axis. However, upon the chemical reduction of Ag^+ by $NaBH_4$, a partial restoration of the i-motif structure was seen (Fig. 1H, solid line), allowing encapsulation and stabilization of the as-formed AgNCs within the interior of the hydrophobic i-motif. Indeed, i-motif structures in DNA sequences with repeated C_4 units have been shown to successfully template the synthesis of photoluminescent AgNCs.[76]

These CD spectroscopic studies have unravelled the important aspects of designing DNA templates for the formation of bright photoluminescent AgNCs. Specifically, two key prerequisites have been established. Firstly, strong binding affinity of the nucleobase to Ag^+ is necessary to hold the metal cation in close proximity for an efficient interaction with the DNA bases upon chemical reduction. This process reduces the probability of forming non-emissive silver nanoparticles of larger sizes (>2 nm). Secondly, self-assembly of DNA molecules into supramolecular structures that can interact with silver atoms and encapsulate the as-formed AgNCs within DNA cages is necessary, thereby stabilizing them against photoluminescence quenching. Indeed, recent crystallographic evidence of AgNCs templated by a DNA decamer reveals very tight binding of the AgNCs within the hydrophobic interior of the DNA structure, completely shielded from the surrounding aqueous environment.[77] Thus, DNA templates that are unable to fulfill the aforementioned criteria such as dT_{20} and dA_{20} as demonstrated herein were unable to form bright emissive AgNCs in solution.

To better understand the color change mechanism of bright emissive dC_{20}-AgNCs and photoluminescence decay of dG_{20}-AgNCs as observed over time, as shown in Fig. 1G and E respectively, detailed structural studies of DNA templates and the atomic number of AgNCs were further investigated using

CD spectroscopy and electrospray ionization (ESI) mass spectroscopy (MS). The time course CD spectra of dC_{20}-AgNCs over 24 hours revealed that the color-conversion phenomenon is accompanied by increasing disruption of the i-motif structure of dC_{20} (ESI Fig. S1†), which is similar to the structural change of the dC_{20} template interacting with Ag^+ (Fig. 1H, dotted line). This observation strongly suggests that increasing quantities of Ag^+ are produced during AgNC aging. The ESI mass spectrum obtained 24 hours after the addition of $NaBH_4$ for AgNC formation showed the presence of multiple species ranging from 6 to 10 Ag atoms per nanocluster (ESI Fig. S2†). The driving force of this conversion has been attributed to the oxidative decomposition of AgNCs by atmospheric oxygen.[78–80]

In a similar way, dG_{20}-AgNCs may also be subjected to oxidative decomposition by oxygen in the air to generate Ag^+ ions, which can in turn disrupt the G-quadruplex structure of dG_{20} templates. The CD spectra of dG_{20}-AgNCs with increasing ages (ESI Fig. S3†) showed a corresponding increase in prominence of the 275 nm peak, which is the characteristic CD spectra of dG_{20} binding with Ag^+. However, the ESI-MS results showed that the dG_{20}-AgNCs were composed of predominantly 8 Ag atoms per cluster (ESI Fig. S4†), which is different from that observed for the dC_{20}-AgNCs (ESI Fig. S2†). This is consistent with the observation that only a single red-emitting species was present in the solution when exposed to air (Fig. 1E). These results may suggest that the oxidative decomposition of AgNCs in the dG_{20} template occur more extensively than that in the dC_{20} template to form Ag^+. Thus, AgNCs emitting at shorter wavelengths would not be formed and stabilized within the dG_{20} template, presumably due to the large difference in binding affinity between the as-generated Ag^+ and AgNCs to the guanine bases. The effect of decomposition-generated Ag^+ due to the dG_{20}-AgNC oxidation[61] induced structural change of the

DNA template was supported by a titration experiment, where the PL intensity of a freshly-prepared solution of dG_{20}-AgNCs was monitored with increasing quantities of added $AgNO_3$ (Fig. 2). It was found that total quenching of the PL intensity of AgNCs occurred at an approximately 0.25 equivalents of Ag^+ relative to the guanine bases, corresponding to one Ag^+ added for every four guanine bases present in the template. Thus, for every four guanine bases that form a tetrad in the G-quadruplex structure, dimer formation involving any two of them (coordinated by 1 Ag^+) can cause structural disruption to displace any photoluminescent AgNCs present within the template. Based on these results, an oxidation-driven mechanism may be proposed for the decomposition of dG_{20}-AgNCs (inset in Fig. 2). As illustrated in this scheme, the high affinity of Ag^+ to dG_{20} forms the guanine–Ag^+–guanine dimers, which disrupt the G-quadruplex structure by changing the orientation of guanine bases relative to each other and enlarging their separation.[10] This weakens the guanine–AgNC binding interaction and increases the susceptibility of AgNCs to oxidative decomposition and displacement by the released Ag^+ from their binding sites.

2.2. Effects of combining two different nucleotides on the photoluminescence of AgNCs

After the pre-requsites for forming ultrasmall AgNCs by homo-oligonucleotides have been set, systematic investigation was extended to a series of DNA templates containing any combination of two types of nucleobases with a general formula of $5'$-$[dX_{5n}Y_{(20-5n)}]$-$3'$ (where X and Y represent any two of the four possible nucleobases and n is an integer from 0 to 4) to synthesize AgNCs with fine-tuned properties. Fig. 3A shows all the possible combinations of two nucleotides in a 20 nt DNA template (see the complete sequences in ESI Table S1†) and the
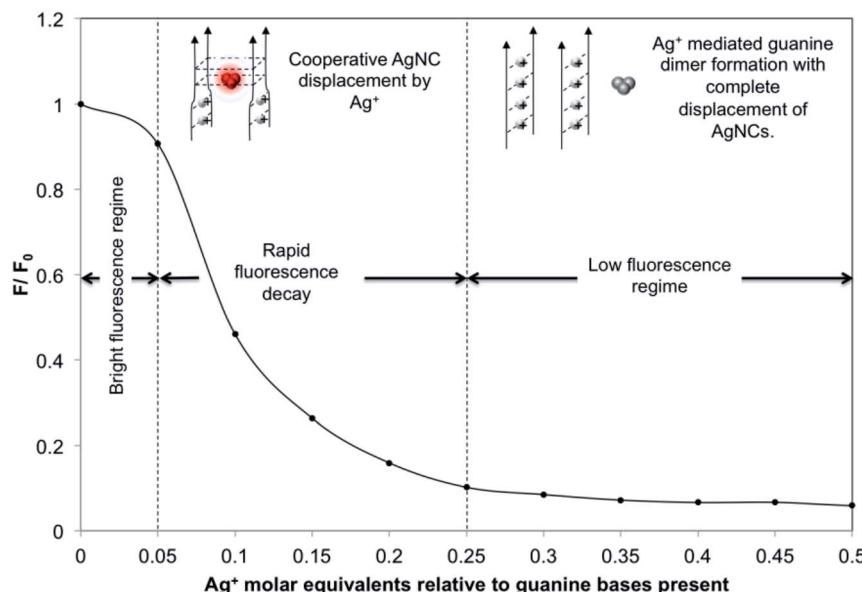

Fig. 2 Photoluminescence (PL) decay curve of the PL quotient (i.e., F during the titration divided by the initial fluorescence F_0) plotted against the quantity of Ag^+ titrated into 50.0 µL of the dG_{20}-templated AgNC solution (relative to the number of moles of guanine bases present in the solution). For this titration, a 0.45 µL aliquot of 2.0 mM $AgNO_3$ solution was added each time.
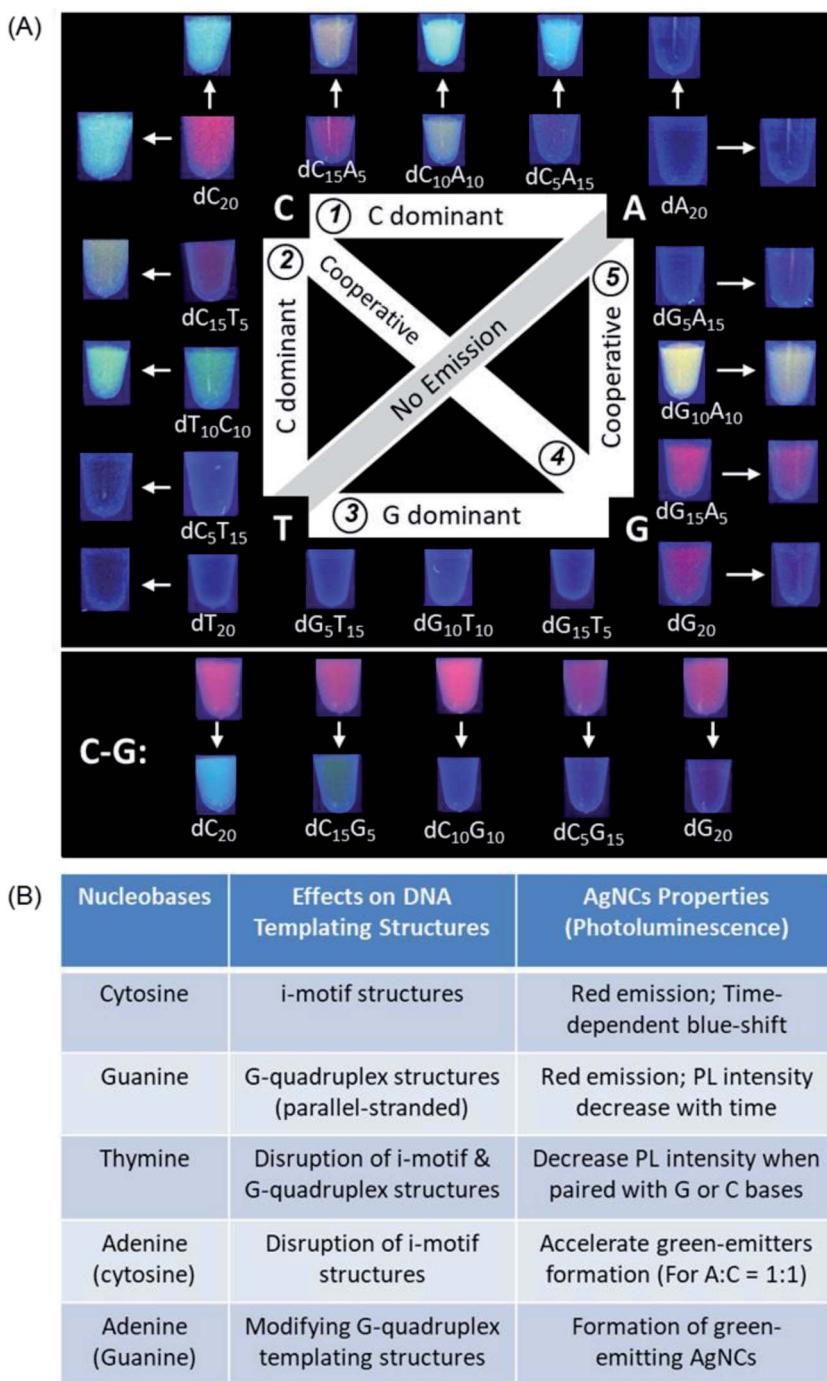
Fig. 3 Summary of the combined nucleobase effects of the DNA templating structures on the formation of photoluminescent AgNCs using systematically varied DNA sequences of 20 nt. (A) Images of the AgNCs formed in the respective DNA sequences under UV light irradiation. Inner and outer images as indicated by arrows show the photoluminescence colours of the freshly synthesized (20 min) and aged (24 h) DNA-templated AgNCs, respectively. Colour photographs of the A–T series are not shown as there is no AgNCs formed. (B) Empirical rules summarized based on (A) to highlight the influence of each nucleotide in a series of 20-mer long DNA templates on the photoluminescence properties of AgNCs.

digital photos of the corresponding DNA-AgNCs under UV light, except for the A–T series which failed to produce any emissive species.

2.2.1. Cytosine dominant effects on C–A and C–T template series. As shown in Fig. 3A, both $[dC_{5n}A_{(20-5n)}]$ (1) and

$[dC_{5n}T_{(20-5n)}]$ (2) series form color changing AgNCs from red to cyan emission within 24 hours (see the photoemission spectra of (1) and (2) in ESI Fig. S5 and S6† respectively), whose results are similar to that observed for the homo-oligonucleotide dC_{20} template. As previously discussed, the red-to-cyan color

conversion is due to the oxidation of red emitters with the simultaneous formation of green- and blue-emitters. This analogy suggests that cytosine exert a dominant influence on the photoluminescence properties of AgNCs synthesized by the C–A series, especially when there are more cytosines in the 2-base DNA templates. The dominating role of cytosine in these DNA sequences is further confirmed by the prevailing i-motif structure as observed in their CD spectra (ESI Fig. S7 and S8†), which is also in line with the fact that cytosine binds more strongly to Ag^+ than adenine and thymine. It should be noted that at a high adenine/thymine content ($\geq 50\%$) relative to cytosine, *e.g.*, $dC_{10}A_{10}$, $dC_{10}T_{10}$ and dC_5T_{15}, the PL intensity of green emitters was competitive to the red-emitting AgNC in 20 min. This result suggests that the inclusion of thymine or adenine in cytosine-containing sequences can promote the formation of green emitters. For adenine, this effect could be attributed to the double-ring purine structure of adenine, which is larger than the single-ring pyrimidine structure of cytosine. Therefore, inclusion of adenine into the cytosine chain can effectively disrupt the templating i-motif structure, which may render the as-formed AgNCs more exposed for oxidative color conversion. Alternatively, changing the identities of the nucleobases binding to the AgNCs can affect their resulting photophysics, as suggested by a recent crystal structure of Ag_8NCs templated by short $5'-A_2C_4-3'$ ssDNA templates, where the green-emitting Ag_8NCs are bound by both ligating nitrogen atoms of cytosine and adenine nucleobases.[81] Similarly, the inclusion of thymine can disrupt the i-motif forming capabilities of oligocytosine sequences (see the CD spectra in ESI Fig. S8†), rendering the as-formed AgNCs less stable to oxidation as well as changing their local coordination environment.

2.2.2. Guanine dominant effects on G–T template series. Similar to the homo-guanine (*i.e.*, dG_{20}, Fig. 1E), the dG_{5n}-$T_{(20-5n)}$ series (3) form the red-emitting AgNCs, whose PL intensity decreases with time (see their photoemission spectra in ESI Fig. S9†), implying the guanine dominant effects on the photoluminescence properties of AgNCs in the G–T series (Fig. 3A). CD spectra also show the presence of the G-quadruplex structure of guanine in the guanine–thymine sequences (ESI Fig. S10†), further confirming the dominant role of guanine. The weaker PL intensity of red-emitting AgNCs with increasing percentage of thymine most likely arises from a fewer guanine nucleobases present in the mixed-base DNA template capable of binding to the AgNCs, causing greater disruption to the stabilizing G-quadruplex structures which are necessary for AgNC formation within (ESI Fig. S10†).

2.2.3. Cooperative effects on C–G and G–A template series. As shown in Fig. 3A, all the $[dC_{5n}G_{(20-5n)}]$ (4) templated AgNCs showed red emission in the first 0.3 hour upon reduction (see the photoemission spectra in ESI Fig. S11†). However, different C/G dominating behaviors were observed over time when the composition of DNA templates varied from $dC_{15}G_5$ to dC_5G_{15} (decreasing the cytosine content from 75% to 25%). When cytosine is the dominant base (C > 50%), the AgNCs underwent color conversions from red to cyan at 24 h, while they remained red-emitting when guanine is dominant (C < 50%). As both cytosine and guanine bind strongly to Ag^+ and can form specific

supramolecular structures to template AgNCs, it is expected that both bases will exert an influence on their photoluminescence properties. The CD spectra of C–G templates clearly show their cooperative effects, where both i-motif and G-quadruplex structures are present in the DNA sequences (ESI Fig. S12†). In addition, the intensity of the CD signal arising from each secondary structure is also proportional to the number of respective bases present. Similarly, both red and green emitters are formed when adenine is included in the $[dG_{5n}A_{(20-5n)}]$ DNA templates (5), where the green emitter can be attributable to the inclusion of adenine (ESI Fig. S13†). While homo-adenine (dA_{20}) was shown to produce weak green emitters (Fig. 1C), the inclusion of guanine bases in the mixed-base DNA template was able to enhance the PL intensity of AgNCs especially when adenine and guanine are present in equimolar quantities (*i.e.*, $dG_{20}A_{20}$ in ESI Fig. S13†), leading to the observation of NC solution with yellow color emission. These results suggest that guanine and adenine exert mutual influence on the photoluminescence properties of AgNCs, which is consistent with the fact that both guanine and adenine exhibited similar binding strength to Ag^+.[67] Furthermore, the CD spectra revealed that both the G-quadruplex and adenine duplex structures are discernible in the DNA templates for G–A series (ESI Fig. S14†).
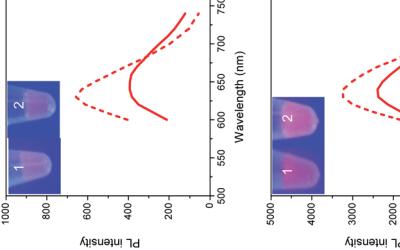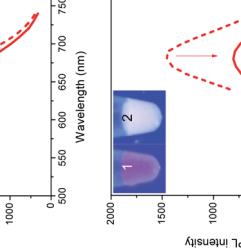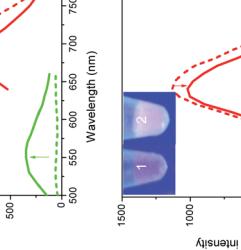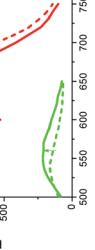
2.2.4. Empirical rules of DNA sequences for tuning the brightness and color emission of AgNCs. In addition to the prerequisite of including cytosine and guanine to generate photoluminescent AgNCs, consecutive sequences of these nucleobases are also important to determine the brightness of DNA-templated AgNCs. As a proof of concept, further experiments were carried out by using interdigitated DNA sequences with the general formula $d(XY)_{10}$ (see the complete sequences in ESI Table S1†) to synthesize AgNCs. The photoluminescence properties of $d(XY)_{10}$-AgNCs were compared to those of those templated by consecutively-linked $dX_{10}Y_{10}$ of the same base composition. As shown in ESI Fig. S15A,† the interdigitated $d(CA)_{10}$, $d(CT)_{10}$, $d(GA)_{10}$ and $d(CG)_{10}$ sequences gave AgNCs with similar emission colors to those produced by their $dX_{10}Y_{10}$ counterparts, but their PL intensities were more than 3 times weaker. CD spectroscopy also revealed that the critical supramolecular structures of DNA templates (*i.e.*, i-motif and G-quadruplex) were not found in the interdigitated sequences, as those functional nucleotides (*e.g.*, cytosine and guanine) are not consecutively distributed despite having the same nucleobase composition as $dX_{10}Y_{10}$ (ESI Fig. S15B†).

Based on the above systematic investigations, we have summarized a set of empirical rules to highlight the influence of each nucleotide in a series of 20-mer long DNA templates on the photoluminescence properties of AgNCs (Fig. 3B). First, cytosine when present as the main component of any two-nucleotide combination (>50%) produces red-emitting AgNCs, which subsequently change to green and blue-emitting species. Second, guanine when present as the main component of any two-nucleotide combination (>50%), produces red-emitting AgNCs with PL intensity decaying with time. Third, both cytosine and guanine in the same sequence show co-dominant effects on the photoluminescence properties of the as-synthesized AgNCs as these two nucleobases bind strongly to

Table 1 Summary of photoluminescence behaviors of AgNCs templated by four aptamers

| No.	Sequence	Percentage of nucleotide present in the sequence/%				Number of consecutive nucleotides present in the sequence				Observation of AgNCs photoluminescence properties
		C	G	A	T	C	G	A	T	
1	5'-ATCTAACTGCTGCGCC GCCGGGAAAATACTGTACGGTTAGA-3' (sgc 8)	24.4	26.8	26.8	22.0	2	2	2	1	
2	5'-AACACCGGGAGGATAGTTCGGTGGCTGTGTTCAGGG TCTCCTCCCGGTG-3' (TDO 5)	25.5	36.2	14.9	23.4	3	6	1	2	
3	5'-ATCTAACTGCTGCGCGCCGCGGGAAAATACTGTACG GTTAGA TTTTTTTTTTCCCCCCCCCCCCCCCCCCCC-3' (sgc 8-T$_{10}$C$_{20}$)	42.3	15.5	15.5	26.8	3	2	2	2	
4	5'-AACACCGGGAGGATAGTTCGGTGGCTGTGTTCAGGG TCTCCTCCCGGTG TTTTTTTTTTCCCCCCCCCCCCCCCCCCCC-3' (TDO 5-T$_{10}$C$_{20}$)	41.6	22.1	9.1	27.3	4	6	1	3	

Ag^+ and are able to form distinct supramolecular structures. Fourth, adenine exerts strong influences on the luminescence of AgNCs when paired with cytosine or guanine, especially in near equal quantities: both $dC_{10}A_{10}$ and $dG_{10}A_{10}$ sequences show notable formation of distinct bright-luminescent green emitters. Finally, thymine alone cannot produce luminescent AgNCs, but can disrupt the supramolecular structure of the DNA template. The combination of thymine and guanine leads to reduced photoluminescence intensity of the resultant AgNC. Contrastingly, thymine–cytosine combinations still allow bright AgNCs to be formed, albeit favouring the production of green emitters.

2.3. Prediction of the photoluminescence colors of aptamer-templated AgNCs for targeted cancer cell imaging

To validate our empirical design rules for predicting the emission color of AgNCs templated by arbitrary DNA sequences, we selected two ssDNA aptamers (sgc 8 and TDO 5 which are known to bind to the human cancer cell lines CEM and Ramos respectively)[82] as DNA templates for AgNC synthesis. The sgc 8 and TDO 5 aptamers have 41 and 47 nucleotides respectively, and both sequences contain guanine as the majority base with consecutive guanine sequences present (Table 1). Thus according to our empirical rules, both sgc 8 and TDO 5 aptamers would be expected to produce red-emissive AgNCs. To modulate the emission colors of AgNCs templated by the selected aptamers, a $T_{10}C_{20}$ sequence was appended to the 3′-terminus of each aptamer (see the complete DNA sequences in Table 1). The T_{10} sequence was introduced as a linker to isolate the NC forming site from the cancer cell targeting sequence, while the C_{20} sequence was introduced to increase the content of cytosine in the modified aptamer such that it is now the dominant base present in the sequence (i.e., 42.3% for sgc 8-$T_{10}C_{20}$ and 41.6% for TDO 5-$T_{10}C_{20}$). As such, the AgNCs templated by both modified aptamer sequences are expected to show a time-dependent photoluminescence color change. However, as the ratio of cytosine to guanine bases present in sgc 8-$T_{10}C_{20}$ is higher
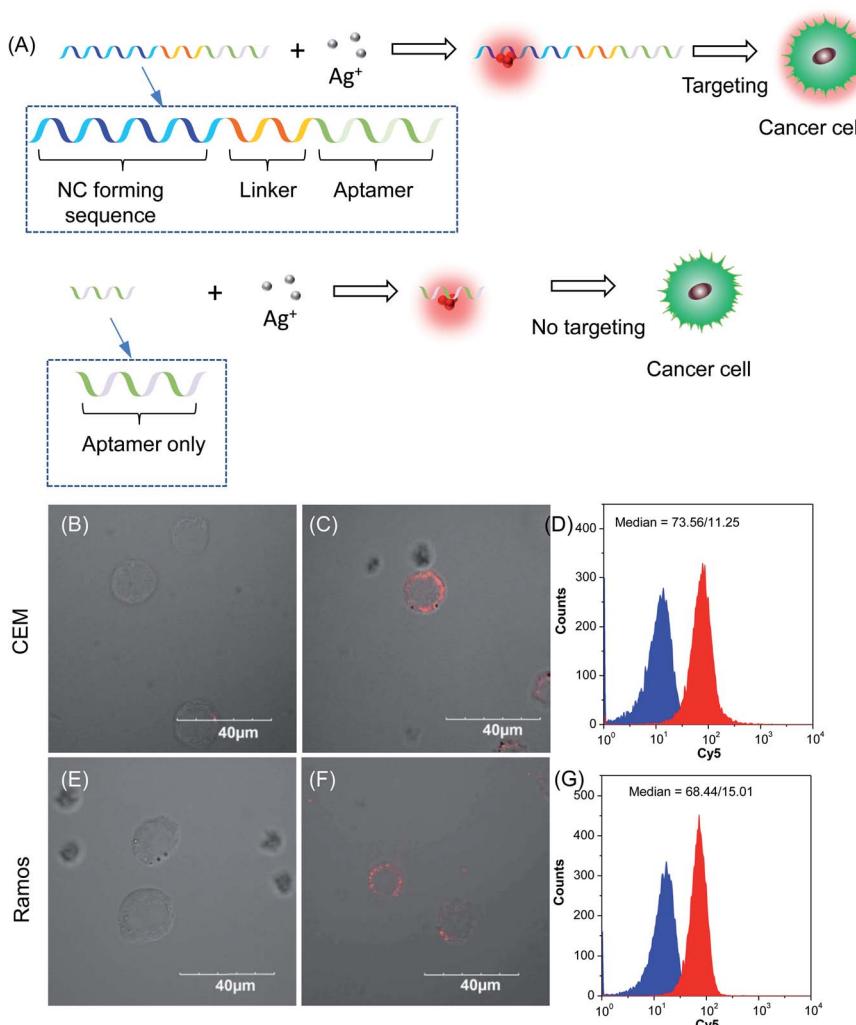
Fig. 4 (A) Schematic diagram of DNA sequence design for cancer diagnostics. Confocal images of (B and C) CEM cells and (E and F) Ramos cells incubated with AgNCs synthesized by using (B and E) unmodified and (C and F) modified sgc 8 (B and C) and TDO 5 (E and F) aptamers as the template. (D, G) Flow cytometry analysis of (D) CEM cells and (G) Ramos cells incubated with AgNCs synthesized by using unmodified (blue) and modified (red) sgc 8 (B and C) and TDO 5 (E and F) aptamers as templates, respectively.

than that for TDO 5-$T_{10}C_{20}$, a greater extent of color change is expected for the former. As predicted, the AgNCs synthesized using sgc 8 and TDO 5 indeed showed red emission ($\lambda_{em} = 645$ nm for sgc 8 and 635 nm for TDO 5) that decayed with time, over 24 hours, which is a characteristic of guanine dominance in the sequence (Table 1). The two modified aptamers indeed caused the change of the emission colors of AgNCs from red (item 1 and dashed lines) to yellow (item 2 and solid lines) with time, due to the formation of green emitters, with a smaller extent of conversion seen for the TDO 5-$T_{10}C_{20}$ as predicted.

For cellular bioimaging and cancer diagnostic applications, the ability of aptamer sequences to specifically target cancer cells is of critical importance. However, the use of unmodified aptamers (e.g. sgc 8 and TDO 5) to template AgNCs may result in the loss of their specific targetting properties due to structural changes associated with AgNC templation and ligation. To address this issue, we hypothesised that introducing an additional AgNC forming sequence which was separated from these aptamers by a linker sequence could preserve the targeting properties, yet retain the ability to form bright-emissive AgNCs for bioimaging (Fig. 4A). To test this hypothesis, we further evaluated the targeting properties of the AgNCs synthesized using original unmodified aptamers (sgc 8 and TDO 5) and modified aptamers (sgc 8-$T_{10}C_{20}$ and TDO 5-$T_{10}C_{20}$) as model templates by confocal laser scanning microscopy and flow cytometry. CEM and Ramos cells were mixed with AgNCs produced by the respective aptamers, i.e., sgc 8 and sgc 8-$T_{10}C_{20}$ for CEM, and TDO 5 and TDO 5-$T_{10}C_{20}$ for Ramos respectively. The corresponding cellular images were examined after four hours of incubation. As shown in Fig. 4B and E, AgNCs synthesized using unmodified aptamers (sgc 8 in B and TDO 5 in E) did not attach to the cell surface, possibly due to the loss of targeting ability during the formation of AgNCs. Those AgNCs synthesized using modified aptamers (sgc 8-$T_{10}C_{20}$ and TDO 5-$T_{10}C_{20}$), however, attach very well on the surface of respective cancer cells (Fig. 4C and F). These results further confirmed the specific targeting properties of AgNCs formed by the modified aptamers for respective cells because of the inclusion of linker sequences that can isolate the NC formation sequence from the targeting sequence to prevent the loss of aptamer specificity. The specific targeting properties of AgNCs synthesized with modified aptamers were further confirmed by flow cytometry. As shown in Fig. 4D and G, the median PL values of CEM and Ramos cells incubated with respective AgNCs templated by modified aptamers (sgc 8-$T_{10}C_{20}$ or TDO 5-$T_{10}C_{20}$ (in red)) were about 6.5-fold and 4.6-fold that of respective cells incubated with AgNCs templated by unmodified aptamers (in blue).

3. Conclusion

In summary, we have conducted systematic investigations of DNA templates (homo-oligonucleotides, combinatorial C–G/C–T/G–A/G–T/C–G/A–T series, interdigitated DNA sequences, and aptamer–NC forming sequences) to unravel the guiding principles in forming AgNCs with fine-tuned photoluminescence properties and functionality. It is revealed that strong base–Ag$^+$ binding and formation of stable supramolecular structures

such as i-motifs and G-quadruplexes are two important prerequisites for forming bright photoluminescent AgNCs. In particular, cytosine and guanine are able to form bright-emissive AgNCs, albeit with very different photoemission behaviors. The former exhibits oxidative color conversion from red to cyan with time, while the latter favors the formation of single red-emitting AgNCs. Altering the DNA sequence with adenine and thymine bases changes the supramolecular structure of DNA templates. The inclusion of adenine bases in DNA templates encourages the formation of green-emitters due to the unique adenine–AgNC bonding interactions, while thymine adversely influences the PL intensity of the resultant AgNCs. In addition, the properties of AgNCs are greatly influenced by the relative base–Ag$^+$ binding affinities, where a large disparity (e.g. C/T and C/A) results in a dominance of the stronger-binding base, while a smaller disparity (e.g. C/G and G/A) allows significant mutual influence and co-dominance. Consecutive sequences of cytosine and/or guanine are also required to form bright emissive AgNCs with strong PL intensity, where these criteria can be used to rationally design suitable DNA sequences for AgNC formation. Based on the empirical rules established from this study, we can predict the luminescence color of AgNCs templated by two arbitrarily selected cancer-cell targeting aptamers. This predictive property was also extended to the modified aptamer sequences, preserving both their specific cellular binding properties and ability to template the formation of photoluminescent AgNCs. Our systematic empirical approach to uncover the design principles of nucleic acid templates for AgNC synthesis complements the existing methodologies towards the ultimate goal of controlling both the photoluminescence and functionalities of DNA-protected AgNCs for multicolor targeted bioimaging applications.

4. Experimental section

4.1. Materials and instrumentation

Silver nitrate (AgNO$_3$, 99.9%) and sodium borohydride (NaBH$_4$, 98%) were purchased from Sigma-Aldrich and used without further purification. All DNA sequences (Sigma Aldrich) were purified by desalting by the manufacturer and used as received without any further purification. Ultrapure water (18 MΩ, prepared from a Millipore Elix 3 purification system) was used throughout the experiment as solvent. Photoluminescence emission spectra were measured on a TECAN infinite M200 plate reader (Tecan Trading AG, Switzerland) using a 384-well black polystyrene microplate (Corning Incorporated, USA) as a sample carrier. All CD measurements were performed using a JASCO J-810 spectrometer in the wavelength range of 200 nm to 350 nm using a 0.1 cm quartz cuvette. Unless otherwise stated, the concentration of DNA used for CD spectroscopy was 3.00 μM, and all AgNC syntheses were carried out as described before dilution for CD measurements.

4.2. Synthesis of silver nanoclusters (AgNCs)

AgNCs were synthesized in the manner reported by Dickson and co-workers[31] based on the optimized base : Ag$^+$: BH$_4^-$ mole ratio

of 2 : 1 : 1. A typical synthesis of dC_{20}-templated AgNCs is as follows: $AgNO_3$ (4.5 µL, 2.00 mM) was added to the dC_{20}-DNA (9.0 µL, 0.10 mM) followed by water (32.0 µL) and vigorously mixed by vortexing for 30 seconds. After standing for 20 minutes, a freshly-prepared aqueous solution of $NaBH_4$ (4.5 µL, 2.00 mM) was added and mixed by vortexing for a further 30 seconds, then the resulting solution was left to incubate at room temperature for 20 minutes. The photoluminescence of the AgNC solution (50.0 µL) was monitored at regular time intervals, and the solution was kept at room temperature in the dark to prevent photo-reduction of Ag^+ between photoluminescence measurements.

4.3. Cellular uptake assay

For confocal microscopy experiments, CEM and Ramos cells obtained from ATCC USA were cultured in the RPMI 1640 medium supplemented with 10% fetal bovine serum (FBS) and 100 IU mL^{-1} penicillin–streptomycin and incubated at 37 °C in a humidified incubator containing 5% wt/vol CO_2. After 80% confluence, cells were fixed with 4% paraformaldehyde and seeded in an 8 well-chamber (LAB-TEK, Chambered Coverglass System) at 1×10^5 cells per mL with incubation of AgNCs at a Ag^+ concentration of 180 µM for 4 h and then the samples were observed under a confocal microscope (Olympus Fluoview FV1000). The images obtained were analyzed using Olympus FV10-ASW imaging software. For flow cytometry measurements, CEM and Ramos cells (2×10^5 cells per well in 24-well plates) were fixed with 4% paraformaldehyde and co-incubated with AgNCs overnight. After incubation, the cells were washed with PBS thrice to remove the free AgNCs, and then the cells were resuspended in 0.5 mL of $1\times$ PBS for flow cytometry measurements. The Cy5 channel ($\lambda_{em} = 570 - 750$ nm) was selected to collect the photoluminescence signal.

Conflicts of interest

There are no conflicts to declare.

Acknowledgements

References

1 Y.-J. Chen, B. Groves, R. A. Muscat and G. Seelig, Nat. Nanotechnol., 2015, 10, 748–760.

2 F. Hong, F. Zhang, Y. Liu and H. Yan, Chem. Rev., 2017, 117, 12584–12640.

3 H. M. Pendergraff, P. M. Krishnamurthy, A. J. Debacker, M. P. Moazami, V. K. Sharma, L. Niitsoo, Y. Yu, Y. N. Tan, H. M. Haitchi and J. K. Watts, Mol. Ther.–Nucleic Acids, 2017, 8, 158–168.

4 N. C. Seeman and H. F. Sleiman, Nat. Rev. Mater., 2017, 3, 17068.

5 H. V. Xu, X. T. Zheng, C. Wang, Y. Zhao and Y. N. Tan, ACS Appl. Nano Mater., 2018, 1, 2062–2068.

6 H. V. Xu, X. T. Zheng, Y. Zhao and Y. N. Tan, ACS Appl. Mater. Interfaces, 2018, 10, 19881–19888.

7 X. T. Zheng, Y. C. Lai and Y. N. Tan, Nanoscale Adv., 2019, 1, 2250–2257.

8 Y. Choi, X. T. Zheng and Y. N. Tan, Mol. Syst. Des. Eng., 2020, 5, 67–90.

9 H. V. Xu, Y. Zhao and Y. N. Tan, ACS Appl. Mater. Interfaces, 2019, 11, 27233–27242.

10 J. Wu, Y. Fu, Z. He, Y. Han, L. Zheng, J. Zhang and W. Li, J. Phys. Chem. B, 2012, 116, 1655–1665.

11 H. V. Xu, X. T. Zheng, B. Y. L. Mok, S. A. Ibrahim, Y. Yu and Y. N. Tan, J. Mol. Eng. Mater., 2016, 04, 1640003.

12 Y. Yu, B. Y. L. Mok, X. J. Loh and Y. N. Tan, Adv. Healthcare Mater., 2016, 5, 1844–1859.

13 J. Chao, Y. Lin, H. Liu, L. Wang and C. Fan, Mater. Today, 2015, 18, 326–335.

14 A. Heuer-Jungemann and T. Liedl, Trends Chem., 2019, 1, 799–814.

15 S. Julin, S. Nummelin, M. A. Kostiainen and V. Linko, J. Nanopart. Res., 2018, 20, 119.

16 N. Li, Y. Shang, Z. Han, T. Wang, Z.-G. Wang and B. Ding, ACS Appl. Mater. Interfaces, 2019, 11, 13835–13852.

17 L.-L. Li, P. Wu, K. Hwang and Y. Lu, J. Am. Chem. Soc., 2013, 135, 2411–2414.

18 Y. N. Tan, J. Y. Lee and D. I. C. Wang, J. Am. Chem. Soc., 2010, 132, 5677–5686.

19 Z. Wang, L. Tang, L. H. Tan, J. Li and Y. Lu, Angew. Chem., Int. Ed., 2012, 51, 9078–9082.

20 J. Wu, L. H. Tan, K. Hwang, H. Xing, P. Wu, W. Li and Y. Lu, J. Am. Chem. Soc., 2014, 136, 15195–15202.

21 J. Zong, S. L. Cobb and N. R. Cameron, Biomater. Sci., 2017, 5, 872–886.

22 A. Aires, E. Lopez-Martinez and A. L. Cortajarena, Biosensors, 2018, 8, 110.

23 F. Pu, X. Ran, M. Guan, Y. Huang, J. Ren and X. Qu, Nano Res., 2018, 11, 3213–3221.

24 Y. Yu, J. Geng, E. Y. X. Ong, V. Chellappan and Y. N. Tan, Adv. Healthcare Mater., 2016, 5, 2528–2535.

25 Y. Yu, S. Y. New, J. Xie, X. Su and Y. N. Tan, Chem. Commun., 2014, 50, 13805–13808.

26 Y. Zhou, J. Wang, G. Yang, S. Ma, M. Zhang and J. Yang, Anal. Methods, 2019, 11, 733–738.

27 Y. Yu, W. D. Lee and Y. N. Tan, Mater. Sci. Eng., C, 2020, 109, 110525.

28 E. Assah, W. Goh, X. T. Zheng, T. X. Lim, J. Li, D. Lane, F. Ghadessy and Y. N. Tan, Colloids Surf., B, 2018, 169, 214–221.

29 B. Shen, V. Linko, K. Tapio, M. A. Kostiainen and J. J. Toppari, Nanoscale, 2015, 7, 11267–11272.

30 X. T. Zheng, W. L. Goh, P. Yeow, D. P. Lane, F. J. Ghadessy and Y. N. Tan, Sens. Actuators, B, 2019, 279, 79–86.

31 J. T. Petty, J. Zheng, N. V. Hud and R. M. Dickson, *J. Am. Chem. Soc.*, 2004, **126**, 5207–5212.

32 Y. S. Ang, W. W. E. Woon and L.-Y. L. Yung, *Nucleic Acids Res.*, 2018, **46**, 6974–6982.

33 Y. Chen, M. L. Phipps, J. H. Werner, S. Chakraborty and J. S. Martinez, *Acc. Chem. Res.*, 2018, **51**, 2756–2763.

34 J. C. Léon, D. González-Abradelo, C. A. Strassert and J. Müller, *Chem.–Eur. J.*, 2018, **24**, 8320–8324.

35 S. Y. New, S. T. Lee and X. D. Su, *Nanoscale*, 2016, **8**, 17729–17746.

36 J. M. Obliosca, C. Liu and H.-C. Yeh, *Nanoscale*, 2013, **5**, 8443–8461.

37 S. Choi, R. M. Dickson and J. Yu, *Chem. Soc. Rev.*, 2012, **41**, 1867–1891.

38 J. Yang, E. Sargent, S. Kelley and J. Y. Ying, *Nat. Mater.*, 2009, **8**, 683–689.

39 Ö. Dag, E. J. Henderson, W. Wang, J. E. Lofgreen, S. Petrov, P. M. Brodersen and G. A. Ozin, *J. Am. Chem. Soc.*, 2011, **133**, 17454–17462.

40 G. De Cremer, B. F. Sels, J.-i. Hotta, M. B. J. Roeffaers, E. Bartholomeeusen, E. Coutiño-Gonzalez, V. Valtchev, D. E. De Vos, T. Vosch and J. Hofkens, *Adv. Mater.*, 2010, **22**, 957–960.

41 M. El-Roz, I. Telegeiev, N. E. Mordvinova, O. I. Lebedev, N. Barrier, A. Behilil, M. Zaarour, L. Lakiss and V. Valtchev, *ACS Appl. Mater. Interfaces*, 2018, **10**, 28702–28708.

42 L. Shang and S. Dong, *Chem. Commun.*, 2008, (9), 1088–1090.

43 Z. Yuan, N. Cai, Y. Du, Y. He and E. S. Yeung, *Anal. Chem.*, 2014, **86**, 419–426.

44 J. Zheng and R. M. Dickson, *J. Am. Chem. Soc.*, 2002, **124**, 13982–13983.

45 I. Chakraborty, S. Mahata, A. Mitra, G. De and T. Pradeep, *Dalton Trans.*, 2014, **43**, 17904–17907.

46 C. P. Joshi, M. S. Bootharaju, M. J. Alhilaly and O. M. Bakr, *J. Am. Chem. Soc.*, 2015, **137**, 11578–11581.

47 R. Yu, N. Lin, W. Yu and X. Y. Liu, *CrystEngComm*, 2015, **17**, 7986–8010.

48 Z. Wu, E. Lanni, W. Chen, M. E. Bier, D. Ly and R. Jin, *J. Am. Chem. Soc.*, 2009, **131**, 16672–16674.

49 J. Yan, H. Su, H. Yang, S. Malola, S. Lin, H. Häkkinen and N. Zheng, *J. Am. Chem. Soc.*, 2015, **137**, 11880–11883.

50 Q. Yao, Y. Yu, X. Yuan, Y. Yu, D. Zhao, J. Xie and J. Y. Lee, *Angew. Chem., Int. Ed.*, 2015, **54**, 184–189.

51 J. Zheng, C. Zhang and R. M. Dickson, *Phys. Rev. Lett.*, 2004, **93**, 077402.

52 S. Pal, R. Varghese, Z. Deng, Z. Zhao, A. Kumar, H. Yan and Y. Liu, *Angew. Chem., Int. Ed.*, 2011, **50**, 4176–4179.

53 Y. Cui, Y. Wang, R. Liu, Z. Sun, Y. Wei, Y. Zhao and X. Gao, *ACS Nano*, 2011, **5**, 8684–8689.

54 S. Roy, A. Baral and A. Banerjee, *ACS Appl. Mater. Interfaces*, 2014, **6**, 4050–4056.

55 J. Yu, S. A. Patel and R. M. Dickson, *Angew. Chem., Int. Ed.*, 2007, **46**, 2028–2030.

56 W. Gong, P. Das, S. Samanta, J. Xiong, W. Pan, Z. Gu, J. Zhang, J. Qu and Z. Yang, *Chem. Commun.*, 2019, **55**, 8695–8704.

57 R. Hardman, *Environ. Health Perspect.*, 2006, **114**, 165–172.

58 F. M. Winnik and D. Maysinger, *Acc. Chem. Res.*, 2013, **46**, 672–680.

59 C. M. Ritchie, K. R. Johnsen, J. R. Kiser, Y. Antoku, R. M. Dickson and J. T. Petty, *J. Phys. Chem. C*, 2007, **111**, 175–181.

60 S. M. Copp, D. Schultz, S. Swasey, J. Pavlovich, M. Debord, A. Chiu, K. Olsson and E. Gwinn, *J. Phys. Chem. Lett.*, 2014, **5**, 959–963.

61 S. Walczak, K. Morishita, M. Ahmed and J. Liu, *Nanotechnology*, 2014, **25**, 155501.

62 C. I. Richards, S. Choi, J.-C. Hsiang, Y. Antoku, T. Vosch, A. Bongiorno, Y.-L. Tzeng and R. M. Dickson, *J. Am. Chem. Soc.*, 2008, **130**, 5038–5039.

63 S. M. Swasey, S. M. Copp, H. C. Nicholson, A. Gorovits, P. Bogdanov and E. G. Gwinn, *Nanoscale*, 2018, **10**, 19701–19705.

64 S. M. Copp, P. Bogdanov, M. Debord, A. Singh and E. Gwinn, *Adv. Mater.*, 2014, **26**, 5839–5845.

65 S. M. Copp, A. Gorovits, S. M. Swasey, S. Gudibandi, P. Bogdanov and E. G. Gwinn, *ACS Nano*, 2018, **12**, 8240–8247.

66 P. R. O'Neill, L. R. Velazquez, D. G. Dunn, E. G. Gwinn and D. K. Fygenson, *J. Phys. Chem. C*, 2009, **113**, 4229–4233.

67 S. Shukla and M. Sastry, *Nanoscale*, 2009, **1**, 122–127.

68 Ö. Persil, C. T. Santai, S. S. Jain and N. V. Hud, *J. Am. Chem. Soc.*, 2004, **126**, 8644–8645.

69 J. Kypr, I. Kejnovská, D. Renčiuk and M. Vorlíčková, *Nucleic Acids Res.*, 2009, **37**, 1713–1725.

70 W. Li, L. Liu, Y. Fu, Y. Sun, J. Zhang and R. Zhang, *Photochem. Photobiol. Sci.*, 2013, **12**, 1864–1872.

71 Y. Fu, J. Zhang, X. Chen, T. Huang, X. Duan, W. Li and J. Wang, *J. Phys. Chem. C*, 2011, **115**, 10370–10379.

72 G. Tao, Y. Chen, R. Lin, J. Zhou, X. Pei, F. Liu and N. Li, *Nano Res.*, 2018, **11**, 2237–2247.

73 S. M. Swasey, L. E. Leal, O. Lopez-Acevedo, J. Pavlovich and E. G. Gwinn, *Sci. Rep.*, 2015, **5**, 10163.

74 D. Zikich, K. Liu, L. Sagiv, D. Porath and A. Kotlyar, *Small*, 2011, **7**, 1029–1034.

75 A. Ono, S. Cao, H. Togashi, M. Tashiro, T. Fujimoto, T. Machinami, S. Oda, Y. Miyake, I. Okamoto and Y. Tanaka, *Chem. Commun.*, 2008, (39), 4825–4827.

76 B. Sengupta, K. Springer, J. G. Buckman, S. P. Story, O. H. Abe, Z. W. Hasan, Z. D. Prudowsky, S. E. Rudisill, N. N. Degtyareva and J. T. Petty, *J. Phys. Chem. C*, 2009, **113**, 19518–19524.

77 C. Cerretani, H. Kanazawa, T. Vosch and J. Kondo, *Angew. Chem., Int. Ed.*, 2019, **58**, 17153–17157.

78 M. R. Carro Temboury, V. Paolucci, E. N. Hooley, L. Latterini and T. Vosch, *Analyst*, 2016, **141**, 123–130.

79 S. Choi, S. Park, K. Lee and J. Yu, *Chem. Commun.*, 2013, **49**, 10908–10910.

80 X. Yuan, Z. Luo, Q. Zhang, X. Zhang, Y. Zheng, J. Y. Lee and J. Xie, *ACS Nano*, 2011, **5**, 8800–8808.

81 D. J. E. Huard, A. Demissie, D. Kim, D. Lewis, R. M. Dickson, J. T. Petty and R. L. Lieberman, *J. Am. Chem. Soc.*, 2019, **141**, 11465–11470.

82 X. Chen, M. C. Estévez, Z. Zhu, Y.-F. Huang, Y. Chen, L. Wang and W. Tan, *Anal. Chem.*, 2009, **81**, 7009–7014.